2-12-2015

Radiative Energy and Momentum Transfer for Various Spherical Shapes: A Single Sphere, a Bubble, a Spherical Shell and a Coated Sphere

Yi Zheng
University of Rhode Island, zheng@uri.edu

Alok Ghanekar

Radiative Energy and Momentum Transfer for Various Spherical Shapes: A Single Sphere, a Bubble, a Spherical Shell and a Coated Sphere

Radiative energy and momentum transfer for various spherical shapes: A single sphere, a bubble, a spherical shell and a coated sphere

Yi Zheng[*] and Alok Ghanekar
Department of Mechanical, Industrial and Systems Engineering,
University of Rhode Island, Kingston, RI 02881, USA

We use fluctuational electrodynamics to determine spectral emissivity and van der Waals contribution to surface energy for various spherical shapes, such as a sphere, a bubble, a spherical shell and a coated sphere, in a homogeneous and isotropic medium. The dyadic Green's function formalism of radiative energy and fluctuation-induced van der Waals stress for different spherical configurations have been developed. We show (1) emission spectra of micro and nano-sized single and coated spheres display several emissivity sharp peaks as the size of object reduces, and (2) surface energy becomes size dependent due to van der Waals phenomena when size of object is reduced to a nanoscopic length scale.

I. INTRODUCTION

Quantum and thermal fluctuations of electromagnetic fields, which give rise to Planck's law of blackbody radiation [1], are responsible for radiative energy, momentum and entropy transfer [2–12]. Classical theory of thermal radiation takes only propagating waves into consideration. Presence of evanescent waves nearby the surfaces leads to near-field effects, such as interference, diffraction and tunneling of surface waves, which are important when the size and length scale is comparable to the thermal wavelength of objects ($\approx 10~\mu$m at room temperature 300 K). Thermal radiation due to fluctuations of electromagnetic fields for a single and/or coated object has been investigated well over the past few decades. For example, Rytov investigated the thermal radiation of a spherical body based on his proposed formalism of electromagnetic fluctuations [2], Eckhardt summerized and compared two methods, Rytov's fluctuation-dissipation theorem and Langevin theory (stochastic electrodynamics) to study the radiative heat transfer [13], Kattawar and Eisner used Rytov's formalism to calculate the radiant power from a homogeneous isothermal sphere of arbitrary size [14], Kruger et al. discussed radiative heat transfer and Casimir force from a cylinder emphasizing its polarized nature [15], Golyk et al. explored the radiation from a long cylinder at uniform temperature when the radius of the cylinder is much smaller than the thermal wavelength [16], Barabanenkov et al. explored the coherent effect of thermal microwave radiation from a heated body [17], and others [18–22]. Near-field radiative energy and momentum transfer between flat and curved surfaces have been studied for the past years. Enhancement of radiative energy transfer, wavelength selectivity, and size and scale dependence are typical characteristics of near-field phenomena which make it more interesting. These characteristics could be exploited in many potential nanotechnological applications such as nanoparticles [23–26] and wavelength selective absorber and emitters

[27–31]. Fluctuations in electromagnetic fields due to the presence of boundaries create van der Waals pressures which lead to momentum transfer [32–35]. These phenomena can be described by cross-spectral densities of the electromagnetic field using dyadic Green's functions of vector Helmholtz equation [36–38]. Such a relation between near-field radiative energy and momentum transfer for arbitrarily shaped objects has been explicitly derived in Ref. [37].

During the past decades, many theoretical works have been published on the topic of the enhanced thermal radiation due to near-field effects and fluctuation-induced van der Waals pressures. Most of them are focused on the configurations, for example, between planar multilayered structures [39–43], coated planar surface [44], photonic multilayer crystals [45–47], gratings [48, 49], cylindrical objects [50, 51], spheres [23, 52–55], a sphere and a flat plate [26, 55–57], and hyperbolic structures [58–60]. Although considerable amount of work devoted to theoretical and experimental results for near-field radiative energy transfer and momentum transfer between objects of the abovementioned typical geometries, these phenomena for a single object requires a further study and a good understanding when the size of the object is reduced to be comparable or less than the thermal wavelength. To the best of our knowledge, most of the works on an individual body rely directly on Rytov's formalism for fluctuating electromagnetic fields [2]. In this work, we applied Rytov's approach and developed a dyadic Green's function formalism for spectral emissivity and van der Waals contribution to surface energy for micro and nano-sized spherical objects, such as a single sphere, a bubble, a sherical shell and a coated sphere, as shown in Fig. 1.

This paper demonstrates how fluctuational electrodynamics can be used to determine spectral emissivity and van der Waals contribution to surface energy for various shapes in a homogenous and isotropic medium. The dyadic Green's function formalism of radiative heat transfer and van der Waals stress for different spherical configurations has been developed. Size dependence and wavelength selectivity of micro and nano-sized spheres are clearly observed. For small sized objects, the emissiv-

ity spectra show sharp peaks at wavelengths corresponding to characteristics of the material's refractive index. The peaks increase as the size of the object decreases. This is consistent with spectral emissivity calculations done for thin films as in Ref. [31]. The calculations for a spherical bubble show that as radius of the bubble reduces, van der Waals energy contribution to the total surface energy increases and dominates it beyond a critical value.

The paper is arranged as follows. Section II focuses on the theoretical formulations for near-field radiative energy transfer and momentum transfer for a generalized case. Calculations of transmissivity for radiative energy transfer and fluctuation-induced van der Waals pressure are discussed in Sec. II A and Sec. II B, respectively. Using this formalism, the analytical expressions of Mie reflection and transmission coefficients for specific cases of a sphere, a bubble, a spherical shell and a coated sphere in a homogeneous and isotropic medium are obtained in Sec. III. Formulae for calculations of spectral emissivity and van der Waals contribution to surface energy of a spherical body are subsequently derived in Sec. III A and Sec. III B. We recapitulate the paper and states the conclusions in Sec. IV.

II. THEORETICAL FUNDAMENTALS

The fluctuations of electric and magnetic current densities, which give rise to radiative transfer and fluctuation-induced electromagnetic forces, can be described by the fluctuation-dissipation theorem [61–63]:

$$\langle J_p^e(\mathbf{r})J_q^{e*}(\tilde{\mathbf{r}})\rangle = 2\omega\varepsilon_o\varepsilon''\Theta\left(\omega,T\right)\delta(\mathbf{r}-\tilde{\mathbf{r}})\delta_{pq} \quad (1a)$$

$$\langle J_p^m(\mathbf{r})J_q^{m*}(\tilde{\mathbf{r}})\rangle = 2\omega\mu_o\mu''\Theta\left(\omega,T\right)\delta(\mathbf{r}-\tilde{\mathbf{r}})\delta_{pq} \quad (1b)$$

$$\langle J_p^e(\mathbf{r})J_q^{m*}(\tilde{\mathbf{r}})\rangle = 0 \quad (1c)$$

where $\mathbf{r}$ and $\tilde{\mathbf{r}}$ are source position vector and observation position vector, ϵ_o and μ_o are the permittivity and permeability of free space, J_p^e and J_p^m are the Cartesian components $(p, q = 1, 2, 3)$ of the electric and magnetic current densities, $\Theta\left(\omega,T\right) = \dfrac{\hbar\omega}{2}\coth\left(\dfrac{\hbar\omega}{2k_BT}\right)$, ε'' and μ'' are the imaginary parts of the dielectric permittivity and magnetic permeability respectively, J^* is the complex conjugate of J, and $\langle\rangle$ denotes the ensemble average. $2\pi\hbar$ is the Planck constant and k_B is the Boltzmann constant. The presence of δ_{pq} implies that all materials are isotropic, and that of $\delta(\mathbf{r}-\tilde{\mathbf{r}})$ implies that the correlations of sources are local.

The Fourier transforms of the electric and magnetic fields due to thermal sources in any object (volume V_s) are given by [2, 37]

$$\mathbf{E}(\tilde{\mathbf{r}}) = \int_{V_s}[\mathbf{p}(\mathbf{r})\cdot\overline{\overline{\mathbf{G}}}_e(\mathbf{r},\tilde{\mathbf{r}}) - \mathbf{J}^m(\mathbf{r})\cdot\overline{\overline{\mathbf{G}}}_E(\mathbf{r},\tilde{\mathbf{r}})]d\mathbf{r} \quad (2a)$$

$$\mathbf{H}(\tilde{\mathbf{r}}) = \int_{V_s}[\mathbf{m}(\mathbf{r})\cdot\overline{\overline{\mathbf{G}}}_m(\mathbf{r},\tilde{\mathbf{r}}) + \mathbf{J}^e(\mathbf{r})\cdot\overline{\overline{\mathbf{G}}}_M(\mathbf{r},\tilde{\mathbf{r}})]d\mathbf{r} \quad (2b)$$

where $\mathbf{p}(\mathbf{r})=i\omega\mu_o\mu(\mathbf{r})\mathbf{J^e}(\mathbf{r})$, $\mathbf{m}(\mathbf{r}) = i\omega\varepsilon_o\varepsilon(\mathbf{r})\mathbf{J^m}(\mathbf{r})$, and, $\varepsilon(\mathbf{r})$ and $\mu(\mathbf{r})$ are the permittivity and permeability at location $\mathbf{r}$. $\overline{\overline{\mathbf{G}}}_E(\mathbf{r},\tilde{\mathbf{r}}) = \nabla\times\overline{\overline{\mathbf{G}}}_e(\mathbf{r},\tilde{\mathbf{r}})$ and $\overline{\overline{\mathbf{G}}}_M(\mathbf{r},\tilde{\mathbf{r}}) = \nabla\times\overline{\overline{\mathbf{G}}}_m(\mathbf{r},\tilde{\mathbf{r}})$. $\overline{\overline{\mathbf{G}}}_e(\mathbf{r},\tilde{\mathbf{r}})$ and $\overline{\overline{\mathbf{G}}}_m(\mathbf{r},\tilde{\mathbf{r}})$ are dyadic Green's functions of the vector Helmholtz equation that satisfy the following boundary conditions on the interface between object 1 and object 2. For electric dyadic Green's functions,

$$\hat{\mathbf{n}}_1\times\mu_1\overline{\overline{\mathbf{G}}}_e(\mathbf{r}_1,\tilde{\mathbf{r}}) = \hat{\mathbf{n}}_2\times\mu_2\overline{\overline{\mathbf{G}}}_e(\mathbf{r}_2,\tilde{\mathbf{r}}), \quad (3a)$$

$$\hat{\mathbf{n}}_1\times\overline{\overline{\mathbf{G}}}_E(\mathbf{r}_1,\tilde{\mathbf{r}}) = \hat{\mathbf{n}}_2\times\overline{\overline{\mathbf{G}}}_E(\mathbf{r}_2,\tilde{\mathbf{r}}), \quad (3b)$$

and for magnetic dyadic Green's functions,

$$\hat{\mathbf{n}}_1\times\varepsilon_1\overline{\overline{\mathbf{G}}}_m(\mathbf{r}_1,\tilde{\mathbf{r}}) = \hat{\mathbf{n}}_2\times\varepsilon_2\overline{\overline{\mathbf{G}}}_m(\mathbf{r}_2,\tilde{\mathbf{r}}), \quad (3c)$$

$$\hat{\mathbf{n}}_1\times\overline{\overline{\mathbf{G}}}_M(\mathbf{r}_1,\tilde{\mathbf{r}}) = \hat{\mathbf{n}}_2\times\overline{\overline{\mathbf{G}}}_M(\mathbf{r}_2,\tilde{\mathbf{r}}), \quad (3d)$$

where $\hat{\mathbf{n}}_1$ and $\hat{\mathbf{n}}_2$ are surface normal vectors, and $\mathbf{r}_1$ and $\mathbf{r}_2$ are position vectors of points on either side of interface in volume V_1 and V_2, as $|\mathbf{r}_1 - \mathbf{r}_2| \to 0$.

A. Transmissivity for radiative energy transfer

The steady state radiative heat transfer from object 1 to object 2, $\mathcal{Q}_{1\to2}$, is given by

$$\mathcal{Q}_{1\to2} = -\oint_{S_2}\mathbf{P}(\tilde{\mathbf{r}})\cdot\hat{\mathbf{n}}_2 d\tilde{\mathbf{r}} \quad (4)$$

where $\mathbf{P}(\tilde{\mathbf{r}}) = \langle\mathbf{E}(\tilde{\mathbf{r}},t)\times\mathbf{H}(\tilde{\mathbf{r}},t)\rangle$ is the Poynting vector at $\tilde{\mathbf{r}}\in S_2$ due to thermally fluctuating sources within V_1. The "$-$" sign in front of the surface integral is because $\hat{\mathbf{n}}_2$ is the outward pointing normal on the surface S_2. The components of $\mathbf{P}(\tilde{\mathbf{r}})$ are given by

$$P_i(\tilde{\mathbf{r}}) = \epsilon_{ipq}\langle E_p(\tilde{\mathbf{r}},t)H_q(\tilde{\mathbf{r}},t)\rangle \quad (5)$$

where p, q=1,2,3 are the labels for the Cartesian components of the vector, ϵ_{ipq} is the Levi-Civita symbol, $\langle E_p(\tilde{\mathbf{r}},t)H_q(\tilde{\mathbf{r}},t)\rangle$ is the contribution to $\langle E_p(\tilde{\mathbf{r}},t)H_q(\tilde{\mathbf{r}},t)\rangle$ from sources within V_1. We note that $\langle E_q(\tilde{\mathbf{r}},t)H_p(\tilde{\mathbf{r}},t)\rangle = \int_0^\infty\dfrac{d\omega}{2\pi}\langle E_q(\tilde{\mathbf{r}},\omega)H_p^*(\tilde{\mathbf{r}},\omega)\rangle$. Using Eq. 2a and Eq. 2b, Eq. 4 for $\mathcal{Q}_{1\to2}$ can be re-written as

$$\mathcal{Q}_{1\to2} = \int_0^\infty\dfrac{d\omega}{2\pi}\left[\Theta\left(\omega,T_1\right)-\Theta\left(\omega,T_2\right)\right]\mathcal{T}_{rr}(\omega) \quad (6)$$

where T_1 and T_2 are the absolute temperatures of objects 1 and 2, and $\mathcal{T}_{rr}(\omega)$ is a generalized transmissivity for radiative energy transport between objects 1 and 2. $\mathcal{T}_{rr}(\omega)$ can be expressed exclusively in terms of components of the dyadic Green's functions on the surfaces of objects 1 and 2, which is given by [37]
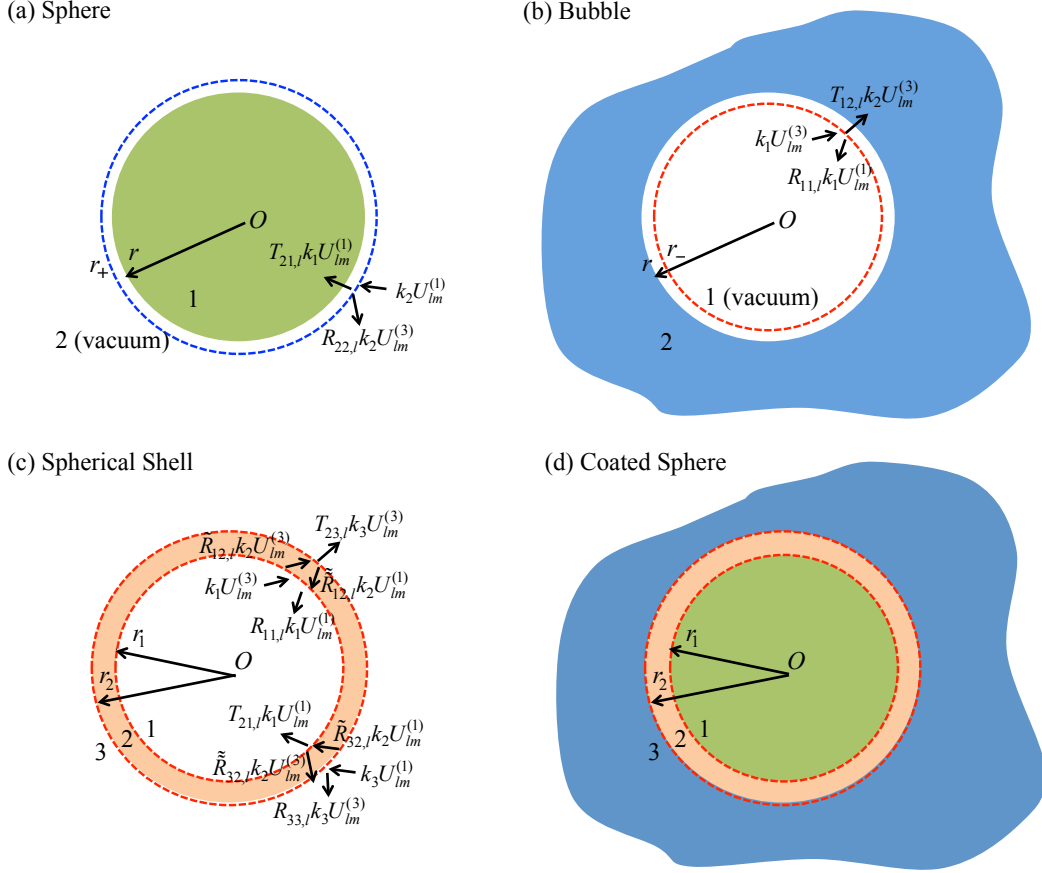
FIG. 1. Schematic of various spherical geometries. (a) a sphere of radius r (material 1, green), (b) a bubble of radius r in material 2 (blue), (c) a spherical shell of interior and exterior radii r_1 and r_2 (material 2, orange), and (d) a sphere of radius r_1 (material 1, green) coated with a thin film of thickness $r_2 - r_1$ (material 2, orange) in material 3 (blue). The short arrows on either side of the interface between two materials denote the spherical electromagnetic waves U ($\boldsymbol{M}$ and $\boldsymbol{N}$ waves). $U_{lm}^{(p)}$ is vector spherical wave functions of order (l, m), and superscript (p) refers to the radial behavior of the waves. k_i is wavenumber in medium i, $R_{ij,l}$ and T_{ij} are the Mie reflection and transmission coefficients due to spherical electromagnetic waves U from medium i to medium j, respectively.

$$\mathcal{T}_{rr}(\omega) = \Re Tr \oint_{S_1} d\mathbf{r} \oint_{S_2} d\tilde{\mathbf{r}} \left[\frac{\omega^2}{c^2} \left[\hat{\mathbf{n}}_2 \times \mu_2 \overline{\overline{G}}_e(\tilde{\mathbf{r}}, \mathbf{r}) \right] \cdot \left[\hat{\mathbf{n}}_1 \times \varepsilon_1^* \overline{\overline{G}}_m^*(\mathbf{r}, \tilde{\mathbf{r}}) \right] + \left[\hat{\mathbf{n}}_2 \times \overline{\overline{G}}_E(\tilde{\mathbf{r}}, \mathbf{r}) \right] \cdot \left[\hat{\mathbf{n}}_1 \times \overline{\overline{G}}_E^*(\mathbf{r}, \tilde{\mathbf{r}}) \right] \right] \quad (7)$$

where $\Re$ stands for the real part, superscript * denotes the complex conjugate, and operator trace $Tr(\overline{\overline{A}}) = \sum_{p=1}^{3} A_{pp}$.

B. van der Waals stress for radiative momentum transfer

Radiative momentum transfer arising from the fluctuations of electromagnetic fields is responsible for the van der Waals pressure, which can be determined from the electromagnetic stress tensor, $\overline{\overline{\sigma}} = \overline{\overline{\sigma}}_e + \overline{\overline{\sigma}}_m$, where $\overline{\overline{\sigma}}_e$ and $\overline{\overline{\sigma}}_m$ are the electric and magnetic field contributions

respectively. Stress tensors $\overline{\overline{\sigma}}_e$ and $\overline{\overline{\sigma}}_m$ are given by [34]

$$\overline{\overline{\sigma}}_e(\tilde{\mathbf{r}}) = \varepsilon_o \left[\langle \mathbf{E}(\tilde{\mathbf{r}}, t) \mathbf{E}(\tilde{\mathbf{r}}, t) \rangle - \frac{1}{2} \overline{\overline{I}} \langle \mathbf{E}^2(\tilde{\mathbf{r}}, t) \rangle \right] \quad (8a)$$

$$\overline{\overline{\sigma}}_m(\tilde{\mathbf{r}}) = \mu_o \left[\langle \mathbf{H}(\tilde{\mathbf{r}}, t) \mathbf{H}(\tilde{\mathbf{r}}, t) \rangle - \frac{1}{2} \overline{\overline{I}} \langle \mathbf{H}^2(\tilde{\mathbf{r}}, t) \rangle \right], \quad (8b)$$

where $\overline{\overline{I}}$ is the identity matrix, $\langle \mathbf{E}(\tilde{\mathbf{r}}, t) \mathbf{E}(\tilde{\mathbf{r}}, t) \rangle$ and $\langle \mathbf{H}(\tilde{\mathbf{r}}, t) \mathbf{H}(\tilde{\mathbf{r}}, t) \rangle$ are matrices whose components are $\langle E_p(\tilde{\mathbf{r}}, t) E_q(\tilde{\mathbf{r}}, t) \rangle$ and $\langle H_p(\tilde{\mathbf{r}}, t) H_q(\tilde{\mathbf{r}}, t) \rangle$ respectively.

Relying on Rytov's theory of fluctuational electrodynamics [2], the cross-spectral correlations of the electric

and magnetic field components can be written as [37]

$$\left\langle E_i(\tilde{\mathbf{r}},\omega)E_j^*(\tilde{\mathbf{r}},\omega)\right\rangle = \frac{2\omega}{\pi}\mu_0\Theta\left(\omega,T\right)$$
$$\times\,\Im\left[\varepsilon(\omega)\mu(\omega)G_{e,ij}(\tilde{\mathbf{r}},\tilde{\mathbf{r}})\right] \quad (9a)$$

$$\left\langle H_i(\tilde{\mathbf{r}},\omega)H_j^*(\tilde{\mathbf{r}},\omega)\right\rangle = \frac{2\omega}{\pi}\varepsilon_0\Theta\left(\omega,T\right)$$
$$\times\,\Im\left[\varepsilon(\omega)\mu(\omega)G_{m,ij}(\tilde{\mathbf{r}},\tilde{\mathbf{r}})\right] \quad (9b)$$

where $\Im$ denotes the imaginary part. $\varepsilon(\omega)$ and $\mu(\omega)$ are

frequency dependent permittivity and permeability of region in which $\tilde{\mathbf{r}}$ is located. $\sqrt{\varepsilon(\omega)} = n(\omega) + i\kappa(\omega)$ and $\mu(\omega) = 1$. The optical data for n and κ can be obtained from Refs. [64, 65]. The van der Waals pressure on the interior surface of a bubble or the exterior surface of a sphere of radius r in an otherwise homogeneous medium (see Figs. 1a and 1b) can be obtained from the $\hat{r}\hat{r}$ component of the electromagnetic stress tensor, in terms of dyadic Green's functions, which is given by

$$\mathcal{S}_{rr}(r) = \int_0^\infty d\omega\frac{2\omega}{\pi c^2}\Theta\left(\omega,T\right)\Im\left\{\varepsilon(\omega)\mu(\omega)\left[G_{e,\hat{r}\hat{r}}(\boldsymbol{r},\boldsymbol{r})-\frac{1}{2}Tr\overline{\overline{G}}_e(\boldsymbol{r},\boldsymbol{r})+G_{m,\hat{r}\hat{r}}(\boldsymbol{r},\boldsymbol{r})-\frac{1}{2}Tr\overline{\overline{G}}_m(\boldsymbol{r},\boldsymbol{r})\right]\right\} \quad (10)$$

where Tr is the trace of the tensor in the spherical coordinates, that is $Tr\left(\overline{\overline{G}}_p\right) = G_{p,\hat{r}\hat{r}} + G_{p,\hat{\theta}\hat{\theta}} + G_{p,\hat{\phi}\hat{\phi}}$. The integral on the right hand side of Eq. 10 is of the form $\int_{0^+}^\infty d\omega\coth\left(\frac{\hbar\omega}{2k_BT_l}\right)\Im f(\omega)$, in which the function $f(\omega+i\xi)$ is analytic in the upper–half of the complex plane ($\xi > 0$). Since $G\left(\boldsymbol{r},\omega\right)$ is analytic in the upper–half of the complex plane, the integral along the real frequency axis can be transformed into summation over Matsubara frequencies, $i\xi_n = in2\pi k_BT_l/\hbar$, as $-\frac{2\pi k_BT}{\hbar}\sum_{n=0}^\infty{}' f(i\xi_n)$. $\sum_{n=0}^\infty{}'$ indicates that the $n=0$ term is multiplied by $1/2$ [66].

$\mathcal{S}_p\left(r\right)$ can be split into two parts: (1) a part which arises from the dyadic Green's function in an infinite homogeneous medium, and (2) a part which arises from the scattered dyadic Green's function due to the presence of boundaries, as $\mathcal{S}_p\left(r\right) = \mathcal{S}^{(o)}\left(r\right)+\mathcal{S}_p^{(sc)}\left(r\right)$. Since $\mathcal{S}^{(o)}\left(r\right)$ is the stress tensor contribution from the homogeneous medium, there is no distinction between the $p=e$ or $p=m$ contributions. The homogeneous part of dyadic Green's function ($\overline{\overline{G}}_e^{(o)}(\mathbf{r},\tilde{\mathbf{r}})$) on either side of the interface between objects 1 and 2 (as shown in Fig. 1) cancels out, while the scattered part of dyadic Green's function is important, which leads to the dispersion force due to the scattering of fluctuations of electromagnetic fields.

The expressions for $\overline{\overline{G}}_e^{(sc)}(\mathbf{r},\tilde{\mathbf{r}})$ when $\mathbf{r},\tilde{\mathbf{r}}\in V_2$ (Fig. 1a) and $\mathbf{r},\tilde{\mathbf{r}}\in V_1$ (Fig. 1b), respectively, are given by

$$\overline{\overline{G}}_e^{(sc)}(\boldsymbol{r},\tilde{\boldsymbol{r}}) = ik_2\sum_{\substack{m=-l,\\l=0}}^{\substack{l=\infty,\\m=l}}(-1)^m$$
$$\times\left[\begin{array}{l}R_{22,l}^{(M)}\boldsymbol{M}_{l,m}^{(3)}(k_2\boldsymbol{r})\,\boldsymbol{M}_{l,-m}^{(3)}(k_2\tilde{\boldsymbol{r}})+\\R_{22,l}^{(N)}\boldsymbol{N}_{l,m}^{(3)}(k_2\boldsymbol{r})\,\boldsymbol{N}_{l,-m}^{(3)}(k_2\tilde{\boldsymbol{r}})\end{array}\right] \quad (11a)$$

$$\overline{\overline{G}}_e^{(sc)}(\boldsymbol{r},\tilde{\boldsymbol{r}}) = ik_1\sum_{\substack{m=-l,\\l=0}}^{\substack{l=\infty,\\m=l}}(-1)^m$$
$$\times\left[\begin{array}{l}R_{11,l}^{(M)}\boldsymbol{M}_{l,m}^{(1)}(k_1\boldsymbol{r})\,\boldsymbol{M}_{l,-m}^{(1)}(k_1\tilde{\boldsymbol{r}})+\\R_{11,l}^{(N)}\boldsymbol{N}_{l,m}^{(1)}(k_1\boldsymbol{r})\,\boldsymbol{N}_{l,-m}^{(1)}(k_1\tilde{\boldsymbol{r}})\end{array}\right] \quad (11b)$$

where, $R_{ij,l}^{(U)}$ is the Mie reflection coefficient due to the source in region i to the observation in region j due to $U = \boldsymbol{M},\boldsymbol{N}$ waves. When $|\boldsymbol{r}| > |\tilde{\boldsymbol{r}}|$. $k_i = \omega\sqrt{\varepsilon_i(\omega)\mu_i(\omega)}/c$ is the wavenumber in region i ($i = 1, 2, 3$), $\boldsymbol{M}_{l,m}^{(p)}(k_ir)$ and $\boldsymbol{N}_{l,m}^{(p)}(k_ir)$ are vector spherical wave functions of order (l,m), and superscript (p) refers to the radial behavior of the waves, given by [67]

$$\boldsymbol{M}_{l,m}^{(p)}(k_ir) = \frac{z_l^{(p)}(k_ir)}{\sqrt{l(l+1)}}\left(\hat{\theta}\frac{imY_{l,m}}{\sin\theta}-\hat{\phi}\frac{\partial Y_{l,m}}{\partial\theta}\right) \quad (12a)$$

$$\boldsymbol{N}_{l,m}^{(p)}(k_ir) = \hat{r}\frac{z_l^{(p)}(k_ir)}{k_ir}\sqrt{l(l+1)}Y_{l,m}$$
$$+\frac{\xi_l^{(p)}(k_ir)}{\sqrt{l(l+1)}}\left(\hat{\theta}\frac{\partial Y_{l,m}}{\partial\theta}+\hat{\phi}\frac{imY_{l,m}}{\sin\theta}\right)$$

For superscript $p = 1$, both $\boldsymbol{M}$ and $\boldsymbol{N}$ waves are regular vector spherical waves and $z_l^{(1)}$ is the spherical Bessel function of first kind of order l. For superscript $p = 3$, both $\boldsymbol{M}$ and $\boldsymbol{N}$ waves are outgoing spherical waves and $z_l^{(3)}$ is the spherical Hankel function of first kind of order l. $\xi_l^{(p)}$ is first derivative of Bessel (Hankel) function, defined as $x\xi_l^{(p)}(x) = \frac{d}{dx}\left[xz_l^{(p)}(x)\right]$. $Y_{l,m}$ is the spherical harmonic of order (l,m).

III.   RESULTS AND DISCUSSION

The spherical configurations of interest in this paper are shown in Fig. 1. To determine the generalized transmissivity for radiative energy transport (Eq. 7) and van der Waals stress (Eq. 10) for these geometries, we need to find the corresponding electric and/or magnetic dyadic Green's functions, which are expressed in terms of the Mie reflection coefficients. Here, we list boundary conditions of electromagnetic fields (see Eqs. A1 - A6 in Appendix A for further details) to be used to calculate the Mie reflection and transmission coefficients (see Eqs. B1a - B2b in Appendix B for further details) for the four cases: (a) a sphere of radius r, (b) a bubble of radius r, (c) a spherical shell of interior and exterior radii r_1 and r_2, and (d) a sphere of radius r_1 with a coating of thickness $r_2 - r_1$ (the same as case (c) in mathematics).

A.   Spectral emissivity of a single/coated sphere

Now, the Mie scattering coefficients and dyadic Green's functions of a sphere are known. Substituting Eq. B2a - Eq. B2b, or Eqs. B4a - B4d, Eq. 11a and Eq. 11b into Eq. 7 yields the transmissivity between a single sphere of radius r, or a coated sphere of radii r_1 and r_2, and a concentric sphere of infinite large radius $r \to \infty$, which is given by (thermal sources within the sphere $r \in V_1$)

$$\mathcal{T}_{rr}(\omega) = 4\pi r^2 \frac{\omega^2}{c^2} \Re \sum_{l=0}^{l=\infty} (-1)^m (2l+1)$$
$$\times \left(|T_{12,l}^{(M)}|^2 + |T_{12,l}^{(N)}|^2 \right) z_l^{(1)}(k_r) \xi_l^{(1)}(k_1 r) \qquad (13)$$

Equation 13 can be modified for the calculation of the spectral emissivity of a single and/or coated sphere, $\epsilon(\omega) = (\hbar\omega/2\pi)\,\mathcal{T}_{rr}/I_\omega$, and I_ω, that is Planck's specific intensity of a monochromatic plane of frequency ω, is $I_\omega = \hbar\omega^3 / \left[4\pi^2 c^2 \left(\exp(\hbar\omega/k_B T) - 1 \right) \right]$.

Figure 2a shows the refractive index, $n + i\kappa$, of silicon carbide (SiC). The spectral emissivity is plotted for SiC half-space and spheres of different radii of 10 μm, 1 μm and 0.5 μm at room temperature $T = 300$ K in Fig. 2b. The black dotted line shows the spectral emissivity of a half-space, which has a low emissivity ($\epsilon \approx 0.1$) when refractive index $n \approx 0$, that is the wavelength between 0.088 eV and 0.12 eV. It can be observed that, as the radius of sphere reduces, the sharp peaks occurs in the emission spectrum. In Fig. 2b, the emission spectrum (blue curve) starts fluctuating when the sphere size ($r = 10$ μm) is comparable to the thermal wavelength ($\lambda_T = 1.27\hbar c/k_B T$) at room temperature $T = 300$ K; when the sphere size is reduced to 1 μm, the emission spectrum (green curve) occurs an obviously high peak of emissivity $\epsilon = 0.43$ at wavelength 0.092 eV and meanwhile a small peak can also be observed at wavelength 0.113 eV which corresponds to the Reststrahlen band ($n \approx 0$ and $\kappa \gg n$) in the dielectric function (Fig. 2a);
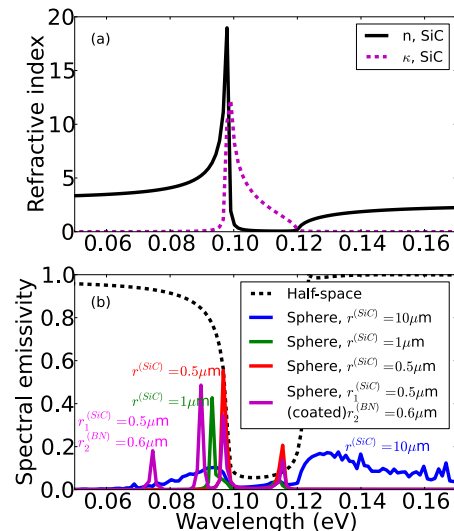

FIG. 2.   Refractive index and spectral emissivity of single/coated SiC spheres of different sizes. (a) real and imaginary parts of the refractive index, $n + i\kappa$, of SiC, and (b) spectral emissivity of a SiC half-space, single SiC spheres of radii 10 μm, 1 μm and 0.5 μm and a SiC sphere ($r_1 = 0.5$ μm) coated with a Boron Nitride (BN) layer of thickness ($r_2 - r_1 = 0.1$ μm) at room temperature $T = 300$ K.

and when radius ($r = 0.5$ μm) is close to the absorption depth ($d_{abs} = c/2\omega\kappa$) of SiC, the emission spectrum (red curve) displays two sharp peaks at wavelengths 0.098 eV and 0.114 eV, respectively. These two emission peaks are exactly corresponding the frequencies at which the dielectric function reaches its minimum value. Other explanation to understand the existence of these sharp peaks in emission spectrum is the absorption depth of electromagnetic waves in comparison to the size of the object. When the radii of spheres become comparable to the absorption depth at mode wavelengths, at which the dielectric functions become negative or very close to zero, the reflection and transmission of a micro/nano-sized sphere are weakened, and the emission is enhanced at those characteristic wavelengths due to multiple reflections and Mie scattering within the object. The emission spectrum of a coated SiC sphere (magenta curve) of radius $r_1 = 0.5$ μm and a Boron Nitride (BN) layer of thickness $r_2 - r_1 = 0.1$ μm displays four sharp peaks. Among them, there are two extra sharp peaks at wavelengths 0.075 eV and 0.089 eV, respectively, which are attributed to a BN thin coating. In comparion with emission spectrum (blue curve) of a single SiC sphere of radius 0.5 μm, it can be seen that the two peaks to the right (magenta curve) occur exactly at the same wavelengths because of sphere core of the same material as well as size. The spectral emissivity can be weakened or strengthened due to a coated thin film or multiple coatings. It requires a good understanding in the further study in future. If the sphere size reduces too much (e.g. $r \lesssim 100$ nm), namely the radius is far less

than the thermal wavelength as well as the penetration depth of electromagnetic waves, most of the waves get reflected or transmitted by the object, like "leakage" to the ambient [1], so the emission spectrum doesn't depend on the wavelength-dependent dielectric function nor the object size strongly.

B. van der Waals surface energy of a spherical bubble

Substituting the scattered part of spherical dyadic Green's functions Eq. 11a and Eq. 11b into Eq. 10, it yields the $\hat{r}\hat{r}$ component of the stress tensor at the interior vacuum-medium interface within a bubble, i.e., at $r \approx r \pm \delta$ as $\delta \to 0$, which can be written as

$$
\mathcal{S}_{rr}(r) = \Re \int\limits_0^\infty d\omega \frac{\hbar\omega^3}{4\pi^2 c^3} \coth\left(\frac{\hbar\omega}{2k_B T}\right) \sum_{l=0}^\infty (2l+1)
$$
$$
\times \left(R_{11,l}^{(M)} + R_{11,l}^{(N)}\right)\left[\left(1 - \frac{l(l+1)}{k_1^2 r^2}\right) z_l^{(1)2}(k_1 r) + \xi_l^{(1)2}(k_1 r)\right]
$$
$$
\tag{14}
$$

Let the hydrostatic pressures in the vacuum and medium out of the bubble be p_V and p_M respectively. Balance of forces at the interface yields a modified Young-Laplace equation, and the pressure change across the interface of a bubble can be expressed below,

$$
\Delta p = p_V - p_M = \mathcal{S}_{rr}(r) + \frac{2\sigma_\infty(T)}{r} \tag{15a}
$$

$$
\Rightarrow \sigma(r,T) \approx \sigma_\infty(T) + \frac{r}{2}\mathcal{S}_{rr}(r) \tag{15b}
$$

where σ_∞ is temperature dependent surface tension. Manipulation of Eq. 15a gives rise to a temperature as well as size dependent surface energy $\sigma(r,T)$ of a bubble of radius r at temperature T in Eq. 15b.

The stress tensor $\mathcal{S}_{rr}(r)$ and surface stress due to surface tension $2\sigma_\infty/r$ are plotted for water and heptane in Fig. 3. The thermophysical property data can be obtained through the NIST Chemistry WebBook [68]. It can be seen that the $\hat{r}\hat{r}$ component of the van der Waals stress obeys a r^{-3} rule, while the stress due to surface tension $2\sigma_\infty/r$ follows r^{-1}. The interaction of two curves implies a critical radius r_{cr} which is defined to be such that $\mathcal{S}_{rr} = 2\sigma_\infty/r$. As $r \gg r_{cr}$, surface tension dominates the surface energy of a bubble in the process of homogeneous nucleation, whereas for $r < r_{cr}$, van der Waals stress plays a significant role in surface energy of a nano-sized bubble. It can be found that the critical radius is $r_{cr} \approx 0.8$ nm for both water and heptane. Eq. 15b shows that surface energy $\sigma(r,T) \approx r\mathcal{S}_{rr}(r)/2$ when $r \ll r_{cr}$, and $\sigma(r,T) \approx \sigma_\infty(T)$ when $r \gg r_{cr}$.
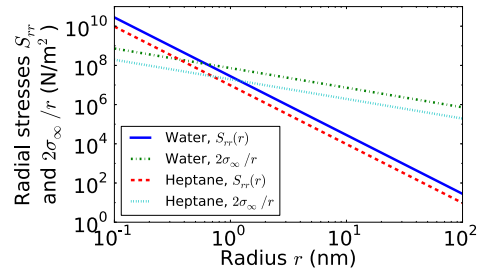

FIG. 3. Size dependence of radial stresses: van der Waals surface stress ($\mathcal{S}_{rr}$) and stress due to surface tension (σ_∞) of a spherical bubble, in water and heptane, respectively. The intersection of the stress lines indicates a critical value of radius r_{cr}, at which the roles of van der Waals stress and surface tension in forming a nano-sized bubble are equal.

IV. CONCLUSION

Fluctuations of electromagnetic fields lead to radiative energy and momentum transfer between objects. They can be described by the cross-spectral densities of the electromagnetic fields, which are expressed in terms of the dyadic Green's functions of the vector Helmholtz equation. The radiative energy and momentum transfer between planar objects have been studied during the past decades, while that between other geometries, such as spherical or cylindrical shapes, have not been investigated well. The proximity approximation and/or modified proximity approximation [69, 70] is one commonly used numerical approach to probe the near-field thermal radiation and fluctuation-induced van der Waals pressure between curved surface, but its validity depends strongly on the configurations and sizes of objects.

In this paper, we apply fluctuational electrodynamics directly to evaluate spectral emissivity of thermal radiation and van der Waals contribution to surface energy for various spherical shapes, such as a sphere, a bubble, a spherical shell and a coated sphere, in a homogeneous and isotropic medium. The dyadic Green's function formalism of thermal radiative transfer and van der Waals stress for different spherical configurations have been developed. We have shown the size dependence and wavelength selectivity of emission spectrum and surface energy of the micro/nanoscale single and coated spheres for small radii. The spectral emissivity of sharp peaks can be observed at wavelengths corresponding to the characteristics of the material's refractive index, and improved as the size of object decreases. van der Waals contribution dominates the surface energy when size of object is reduced to a nanoscopic length scale. The study of fluctuation-induced radiative energy and momentum transfer for spherical shapes has great applications in the nanoscale engineering, e.g., nanobeads, nanoparticle-nanofiber composites and multilayer-coated spherical shells. It deserves further investigation on the study of enhanced wavelength selectivity of radiative

thermal properties of nano-sized particles and the electromagnetic effect of van der Waals contribution to the formation of bubbles in the phase change heat transfer in future.

Appendix A: Boundary conditions of electromagnetic fields for four spherical cases

The boundary conditions of electromagnetic fields are listed below for the four cases: (a) a sphere of radius r, (b) a bubble of radius r, (c) a spherical shell of interior and exterior radii r_1 and r_2, and (d) a sphere of radius r_1 with a coating of thickness $r_2 - r_1$.

Case (a): A sphere with a radius of $r_+ = r + \delta$ ($\delta \to 0$). Thermal sources are outside the sphere, that is $r \in V_2$. The boundary conditions are given by

$$\begin{cases} \mu_2 z_l^{(1)}(k_2 r) + R_{22,l}^{(M)} \mu_2 z_l^{(3)}(k_2 r) = T_{21,l}^{(M)} \mu_1 z_l^{(1)}(k_1 r) \\ k_2 \xi_l^{(1)}(k_2 r) + R_{22,l}^{(M)} k_2 \xi_l^{(3)}(k_2 r) = T_{21,l}^{(M)} k_1 \xi_l^{(1)}(k_1 r) \end{cases} \tag{A1}$$

Case (b): A bubble with a radius of $r_- = r - \delta$ ($\delta \to 0$). Thermal sources are inside the bubble, that is $r \in V_1$. The boundary conditions are given by

$$\begin{cases} \mu_1 z_l^{(3)}(k_1 r) + R_{11,l}^{(M)} \mu_1 z_l^{(1)}(k_1 r) = T_{12,l}^{(M)} \mu_2 z_l^{(3)}(k_2 r) \\ k_1 \xi_l^{(3)}(k_1 r) + R_{11,l}^{(M)} k_1 \xi_l^{(1)}(k_1 r) = T_{12,l}^{(M)} k_2 \xi_l^{(3)}(k_2 r) \end{cases} \tag{A2}$$

Case (c): A spherical shell with an interior radius r_1 and an exterior radius r_2. (or Case (d): A sphere with a radius r_1 coated with a thin film of thickness $r_2 - r_1$. If thermal sources are in material 1 ($r \in V_1$), the boundary conditions at $r = r_1$ are given by

$$\begin{cases} \mu_1 z_l^{(3)}(k_1 r_1) + R_{11,l}^{(M)} \mu_1 z_l^{(1)}(k_1 r_1) = \widetilde{R}_{12,l}^{(M)} \mu_2 z_l^{(3)}(k_2 r_1) + \widetilde{\widetilde{R}}_{12,l}^{(M)} \mu_2 z_l^{(1)}(k_2 r_1) \\ k_1 \xi_l^{(3)}(k_1 r_1) + R_{11,l}^{(M)} k_1 \xi_l^{(1)}(k_1 r_1) = \widetilde{R}_{12,l}^{(M)} k_2 \xi_l^{(3)}(k_2 r_1) + \widetilde{\widetilde{R}}_{12,l}^{(M)} k_2 \xi_l^{(1)}(k_2 r_1) \end{cases} \tag{A3}$$

and the boundary conditions at $r = r_2$ are given by

$$\begin{cases} \widetilde{R}_{12,l}^{(M)} \mu_2 z_l^{(3)}(k_2 r_2) + \widetilde{\widetilde{R}}_{12,l}^{(M)} \mu_2 z_l^{(1)}(k_2 r_2) = T_{23,l}^{(M)} \mu_3 z_l^{(3)}(k_3 r_2) \\ \widetilde{R}_{12,l}^{(M)} k_2 \xi_l^{(3)}(k_2 r_2) + \widetilde{\widetilde{R}}_{12,l}^{(M)} k_2 \xi_l^{(1)}(k_2 r_2) = T_{23,l}^{(M)} k_3 \xi_l^{(3)}(k_3 r_2) \end{cases} \tag{A4}$$

And, if thermal sources are in material 3 ($r \in V_3$), the boundary conditions at $r = r_2$ are given by

$$\begin{cases} \mu_3 z_l^{(1)}(k_3 r_2) + R_{33,l}^{(M)} \mu_3 z_l^{(3)}(k_3 r_2) = \widetilde{R}_{32,l}^{(M)} \mu_2 z_l^{(1)}(k_2 r_2) + \widetilde{\widetilde{R}}_{32,l}^{(M)} \mu_2 z_l^{(3)}(k_2 r_2) \\ k_3 \xi_l^{(1)}(k_3 r_2) + R_{33,l}^{(M)} k_3 \xi_l^{(3)}(k_3 r_2) = \widetilde{R}_{32,l}^{(M)} k_2 \xi_l^{(1)}(k_2 r_2) + \widetilde{\widetilde{R}}_{32,l}^{(M)} k_2 \xi_l^{(3)}(k_2 r_2) \end{cases} \tag{A5}$$

and the boundary conditions at $r = r_1$ are given by

$$\begin{cases} \widetilde{R}_{32,l}^{(M)} \mu_2 z_l^{(1)}(k_2 r_1) + \widetilde{\widetilde{R}}_{32,l}^{(M)} \mu_2 z_l^{(3)}(k_2 r_1) = T_{21,l}^{(M)} \mu_1 z_l^{(1)}(k_1 r_1) \\ \widetilde{R}_{32,l}^{(M)} k_2 \xi_l^{(1)}(k_2 r_1) + \widetilde{\widetilde{R}}_{32,l}^{(M)} k_2 \xi_l^{(3)}(k_2 r_1) = T_{21,l}^{(M)} k_1 \xi_l^{(1)}(k_1 r_1) \end{cases} \tag{A6}$$

Here, $R_{ij,l}^{(U)}$ and $T_{ij}^{(U)}$ are the Mie reflection and transmission coefficients due to $U(= \boldsymbol{M}, \boldsymbol{N})$ waves from region i to region j, respectively.

Appendix B: Mie reflection and transmission coefficients

For example, the Mie coefficients due to $\boldsymbol{M}$ waves $R_{11,l}^{(M)}$ and $T_{12,l}^{(M)}$ in Case (a) can be obtained from Eq. A1 as

$$R_{22,l}^{(M)} = -\frac{\left(\dfrac{k_2}{\mu_2}\dfrac{\xi_l^{(1)}(k_2 a)}{z_l^{(1)}(k_2 r)} - \dfrac{k_1}{\mu_1}\dfrac{\xi_l^{(1)}(k_1 r)}{z_l^{(1)}(k_1 a)}\right) z_l^{(1)}(k_2 r)}{\left(\dfrac{k_2}{\mu_2}\dfrac{\xi_l^{(3)}(k_2 a)}{z_l^{(3)}(k_2 r)} - \dfrac{k_1}{\mu_1}\dfrac{\xi_l^{(1)}(k_1 r)}{z_l^{(1)}(k_1 a)}\right) z_l^{(3)}(k_2 r)} \tag{B1a}$$

$$T_{21,l}^{(M)} = \frac{\mu_2}{\mu_1}\left(\frac{y_l^{(1)}(k_2 r)}{y_l^{(1)}(k_1 r)} + R_{22,l}^{(M)}\frac{y_l^{(3)}(k_2 r)}{y_l^{(1)}(k_1 r)}\right) \tag{B1b}$$

and the Mie coefficients due to $\boldsymbol{M}$ waves $R_{22,l}^{(M)}$ and $T_{21,l}^{(M)}$ in Case (b) can be obtained from Eq. A2 as

$$R_{11,l}^{(M)} = -\frac{\left(\dfrac{k_1}{\mu_1}\dfrac{\xi_l^{(3)}(k_1 r)}{z_l^{(3)}(k_1 r)} - \dfrac{k_2}{\mu_2}\dfrac{\xi_l^{(3)}(k_2 r)}{z_l^{(3)}(k_2 r)}\right) z_l^{(3)}(k_1 r)}{\left(\dfrac{k_1}{\mu_1}\dfrac{\xi_l^{(1)}(k_1 r)}{z_l^{(1)}(k_1 r)} - \dfrac{k_2}{\mu_2}\dfrac{\xi_l^{(3)}(k_2 r)}{z_l^{(3)}(k_2 r)}\right) z_l^{(1)}(k_1 r)} \tag{B2a}$$

$$T_{12,l}^{(M)} = \frac{\mu_1}{\mu_2}\left(\frac{y_l^{(3)}(k_1 r)}{y_l^{(3)}(k_2 r)} + R_{11,l}^{(M)}\frac{y_l^{(1)}(k_1 r)}{y_l^{(3)}(k_2 r)}\right) \tag{B2b}$$

The Mie reflection and transmission coefficients due to $\boldsymbol{M}$ waves in Cases (c) and (d) can be obtained by solving Eqs. A3 - A6. If thermal sources in material 1 ($r \in V_1$), Eq. A3 and Eq. A4 can be rewritten as

$$\begin{bmatrix} -\mu_1 z_l^{(1)}(k_1 r_1) & \mu_2 z_l^{(3)}(k_2 r_1) & \mu_2 z_l^{(1)}(k_2 r_1) & 0 \\ -k_1 \xi_l^{(1)}(k_1 r_1) & k_2 \xi_l^{(3)}(k_2 r_1) & k_2 \xi_l^{(1)}(k_2 r_1) & 0 \\ 0 & \mu_2 z_l^{(3)}(k_2 r_2) & \mu_2 z_l^{(1)}(k_2 r_2) & -\mu_3 z_l^{(3)}(k_3 r_2) \\ 0 & k_2 \xi_l^{(3)}(k_2 r_2) & k_2 \xi_l^{(1)}(k_2 r_2) & -k_3 \xi_l^{(3)}(k_3 r_2) \end{bmatrix} \begin{bmatrix} R_{11,l}^{(M)} \\ \widetilde{R}_{12,l}^{(M)} \\ \widetilde{\widetilde{R}}_{12,l}^{(M)} \\ T_{23,l}^{(M)} \end{bmatrix} = \begin{bmatrix} \mu_1 z_l^{(3)}(k_1 r_1) \\ k_1 \xi_l^{(3)}(k_1 r_1) \\ 0 \\ 0 \end{bmatrix} \tag{B3}$$

and, it leads to

$$R_{11,l}^{(M)} = -\frac{-NCJE + MCKE + IDNE - DLKE + ANGJ - AMGK - IAHN + ALHK}{-NCFJ + NGBJ - BMGK - IBHN + BHLK + FMCK + IFDN - FDLK} \tag{B4a}$$

$$\widetilde{R}_{12,l}^{(M)} = -\frac{(-EB + AF)(NJ - MK)}{-NCFJ + NGBJ - BMGK - IBHN + BHLK + FMCK + IFDN - FDLK} \tag{B4b}$$

$$\widetilde{\widetilde{R}}_{12,l}^{(M)} = -\frac{(-IN + KL)(-EB + AF)}{-NCFJ + NGBJ - BMGK - IBHN + BHLK + FMCK + IFDN - FDLK} \tag{B4c}$$

$$T_{23,l}^{(M)} = -\frac{(-IM + JL)(-EB + AF)}{-NCFJ + NGBJ - BMGK - IBHN + BHLK + FMCK + IFDN - FDLK} \tag{B4d}$$

where,

$$A = \mu_1 z_l^{(3)}(k_1 r_1), B = \mu_1 z_l^{(1)}(k_1 r_1), C = \mu_2 z_l^{(3)}(k_2 r_1), D = \mu_2 z_l^{(1)}(k_2 r_1), \tag{B5a}$$

$$E = k_1 \xi_l^{(3)}(k_1 r_1), F = k_1 \xi_l^{(1)}(k_1 r_1), G = k_2 \xi_l^{(3)}(k_2 r_1), H = k_2 \xi_l^{(1)}(k_2 r_1), \tag{B5b}$$

$$I = \mu_2 z_l^{(3)}(k_2 r_2), J = \mu_2 z_l^{(1)}(k_2 r_2), K = \mu_3 z_l^{(3)}(k_3 r_2), \tag{B5c}$$

$$L = k_2 \xi_l^{(3)}(k_2 r_2), M = k_2 \xi_l^{(1)}(k_2 r_2), N = k_3 \xi_l^{(3)}(k_3 r_2), \tag{B5d}$$

If thermal sources in material 3 ($r \in V_3$), Eq. A5 and Eq. A6 can be rewritten as

$$\begin{bmatrix} -\mu_3 z_l^{(3)}(k_3 r_2) & \mu_2 z_l^{(1)}(k_2 r_2) & \mu_2 z_l^{(3)}(k_2 r_2) & 0 \\ -k_3 \xi_l^{(3)}(k_3 r_2) & k_2 \xi_l^{(1)}(k_2 r_2) & k_2 \xi_l^{(3)}(k_2 r_2) & 0 \\ 0 & \mu_2 z_l^{(1)}(k_2 r_1) & \mu_2 z_l^{(3)}(k_2 r_1) & -\mu_1 z_l^{(1)}(k_1 r_1) \\ 0 & k_2 \xi_l^{(1)}(k_2 r_1) & k_2 \xi_l^{(3)}(k_2 r_1) & -k_1 \xi_l^{(1)}(k_1 r_1) \end{bmatrix} \begin{bmatrix} R_{33,l}^{(M)} \\ \widetilde{R}_{32,l}^{(M)} \\ \widetilde{\widetilde{R}}_{32,l}^{(M)} \\ T_{21,l}^{(M)} \end{bmatrix} = \begin{bmatrix} \mu_3 z_l^{(1)}(k_3 r_2) \\ k_3 \xi_l^{(1)}(k_3 r_2) \\ 0 \\ 0 \end{bmatrix} \tag{B6}$$

and, it leads to

$$R_{33,l}^{(M)} = -\frac{-NCJE + MCKE + IDNE - DLKE + ANGJ - AMGK - IAHN + ALHK}{-NCFJ + NGBJ - BMGK - IBHN + BHLK + FMCK + IFDN - FDLK} \tag{B7a}$$

$$\widetilde{R}_{32,l}^{(M)} = -\frac{(-EB + AF)(NJ - MK)}{-NCFJ + NGBJ - BMGK - IBHN + BHLK + FMCK + IFDN - FDLK} \tag{B7b}$$

$$\widetilde{\widetilde{R}}_{32,l}^{(M)} = -\frac{(-IN + KL)(-EB + AF)}{-NCFJ + NGBJ - BMGK - IBHN + BHLK + FMCK + IFDN - FDLK} \tag{B7c}$$

$$T_{21,l}^{(M)} = -\frac{(-IM + JL)(-EB + AF)}{-NCFJ + NGBJ - BMGK - IBHN + BHLK + FMCK + IFDN - FDLK} \tag{B7d}$$

where,

$$A = \mu_3 z_l^{(1)}(k_3 r_2), B = \mu_3 z_l^{(3)}(k_3 r_2), C = \mu_2 z_l^{(1)}(k_2 r_2), D = \mu_2 z_l^{(3)}(k_2 r_2), \tag{B8a}$$

$$E = k_3 \xi_l^{(1)}(k_3 r_2), F = k_3 \xi_l^{(3)}(k_3 r_2), G = k_2 \xi_l^{(1)}(k_2 r_2), H = k_2 \xi_l^{(3)}(k_2 r_2), \tag{B8b}$$

$$I = \mu_2 z_l^{(1)}(k_2 r_1), J = \mu_2 z_l^{(3)}(k_2 r_1), K = \mu_1 z_l^{(1)}(k_1 r_1), \tag{B8c}$$

$$L = k_2 \xi_l^{(1)}(k_2 r_1), M = k_2 \xi_l^{(3)}(k_2 r_1), N = k_1 \xi_l^{(1)}(k_1 r_1), \tag{B8d}$$

Similarly, the Mie coefficients due to $\boldsymbol{N}$ waves can be obtained by simply switching functions of z_l and ξ_l [67]. Substituting the Mie coefficients into Eqs. 11a and 11b yields the scattering parts of dyadic Green's functions, and then they can be used to determine a generalized transmissivity for radiative energy transfer (Eq. 7) and an electromagnetic stress tensor (Eq. 10).

[1] M. Planck, *The theory of heat radiation* (Dover Publications, 2011).

[2] S. Rytov, *Theory of Electric Fluctuations and Thermal Radiation (Air Force Cambridge Research Center, Bedford, Mass., 1959)*, Tech. Rep. (AFCRC-TR-59-162, 1967).

[3] D. Polder and M. Van Hove, Physical Review B **4**, 3303 (1971).

[4] J. Eckardt, Physical Review A **18**, 426 (1978).

[5] C. Hargreaves, Physics Letters A **30**, 491 (1969).

[6] J. Inglesfield and J. Pendry, Philosophical Magazine **34**, 205 (1976).

[7] I. Dorofeyev, H. Fuchs, B. Gotsmann, and G. Wenning, Physical Review B **60**, 9069 (1999).

[8] I. Dorofeyev, Journal of Physics D: Applied Physics **31**, 600 (1998).

[9] S. Basu, Z. Zhang, and C. Fu, International Journal of Energy Research **33**, 1203 (2009).

[10] Y. Zheng and A. Narayanaswamy, Physical Review A **89**, 022512 (2014).

[11] M. Francoeur, S. Basu, and S. J. Petersen, Optics express **19**, 18774 (2011).

[12] A. Narayanaswamy and Y. Zheng, Physical Review B **88**, 075412 (2013).

[13] W. Eckhardt, Physical Review A **29**, 1991 (1984).

[14] G. Kattawar and M. Eisner, Applied optics **9**, 2685 (1970).

[15] M. Krüger, T. Emig, and M. Kardar, Physical Review Letters **106**, 210404 (2011).

[16] V. A. Golyk, M. Krüger, and M. Kardar, Physical Review E **85**, 046603 (2012).

[17] Y. N. Barabanenkov and M. Y. Barabanenkov, Bulletin of the Russian Academy of Sciences: Physics **72**, 27 (2008).

[18] Y. Öhman, Nature **192**, 254 (1961).

[19] R. Carminati and J.-J. Greffet, Physical Review Letters **82**, 1660 (1999).

[20] G. Biener, N. Dahan, A. Niv, V. Kleiner, and E. Hasman, Applied Physics Letters **92**, 081913 (2008).

[21] A. E. Aliev and A. A. Kuznetsov, Physics Letters A **372**, 4938 (2008).

[22] Y.-Y. Au, H. S. Skulason, S. Ingvarsson, L. J. Klein, and H. F. Hamann, Physical Review B **78**, 085402 (2008).

[23] A. Pérez-Madrid, J. M. Rubí, and L. C. Lapas, Physical Review B **77**, 155417 (2008).

[24] O. Huth, F. Rüting, S.-A. Biehs, and M. Holthaus, The European Physical Journal Applied Physics **50**, 10603 (2010).

[25] T. Von Werne and T. E. Patten, Journal of the American Chemical Society **121**, 7409 (1999).

[26] S.-A. Biehs and J.-J. Greffet, Physical Review B **81**, 245414 (2010).

[27] E. Rephaeli and S. Fan, Optics express **17**, 15145 (2009).

[28] Y. Avitzour, Y. Urzhumov, and G. Shvets, Phys. Rev. B **79**, 045131 (2009).

[29] N. Sergeant, M. Agrawal, and P. Peumans, Optics Express **18**, 5525 (2010).

[30] L. Cao, P. Fan, A. P. Vasudev, J. S. White, Z. Yu, W. Cai, J. A. Schuller, S. Fan, and M. L. Brongersma, Nano letters **10**, 439 (2010).

[31] A. Narayanaswamy, J. Mayo, and C. Canetta, Applied Physics Letters **104**, 183107 (2014).

[32] V. Belosludov and V. Nabutovskiy, Zh. eksp. i teor. fiz **68**, 2177 (1975).

[33] L. Pitaevskii, Physical Review A **73**, 047801 (2006).

[34] A. Narayanaswamy and Y. Zheng, Physical Review A **88**, 012502 (2013).

[35] V. A. Parsegian, *Van der Waals forces: a handbook for biologists, chemists, engineers, and physicists* (Cambridge University Press, 2006).

[36] C.-T. Tai, *Dyadic Green functions in electromagnetic theory*, Vol. 272 (IEEE press New York, 1994).

[37] A. Narayanaswamy and Y. Zheng, Journal of Quantitative Spectroscopy and Radiative Transfer **132**, 12 (2014).

[38] P. Yla-Oijala and M. Taskinen, Antennas and Propagation, IEEE Transactions on **51**, 2106 (2003).

[39] S. M. Rao, D. Wilton, and A. W. Glisson, Antennas and Propagation, IEEE Transactions on **30**, 409 (1982).

[40] P. Ben-Abdallah, K. Joulain, J. Drevillon, and G. Domingues, Journal of Applied Physics **106**, 044306 (2009).

[41] M. Francoeur, M. Pinar Mengüç, and R. Vaillon, Journal of Quantitative Spectroscopy and Radiative Transfer **110**, 2002 (2009).

[42] V. A. Parsegian and B. W. Ninham, Journal of Theoretical Biology **38**, 101 (1973).

[43] K. Joulain, J.-P. Mulet, F. Marquier, R. Carminati, and J.-J. Greffet, Surface Science Reports **57**, 59 (2005).

[44] S.-A. Biehs, The European Physical Journal B-Condensed Matter and Complex Systems **58**, 423 (2007).

[45] A. Narayanaswamy and G. Chen, Journal of Quantitative Spectroscopy and Radiative Transfer **93**, 175 (2005).

[46] W. T. Lau, J.-T. Shen, G. Veronis, S. Fan, and P. V. Braun, Applied Physics Letters **92**, 103106 (2008).

[47] M. Tschikin, P. Ben-Abdallah, and S.-A. Biehs, Physics Letters A **376**, 3462 (2012).

[48] S.-A. Biehs, F. S. Rosa, and P. Ben-Abdallah, Applied Physics Letters **98**, 243102 (2011).

[49] L. Wang and Z. M. Zhang, JOSA B **27**, 2595 (2010).

[50] M. Sheikholeslami and D. D. Ganji, Journal of the Brazilian Society of Mechanical Sciences and Engineering , 1 (2014).

[51] S. Edalatpour and M. Francoeur, Journal of Quantitative Spectroscopy and Radiative Transfer **133**, 364 (2014).

[52] K. Sasihithlu and A. Narayanaswamy, Physical Review B **83**, 161406 (2011).

[53] L. Zhu, C. R. Otey, and S. Fan, Physical Review B **88**, 184301 (2013).

[54] A. Narayanaswamy, S. Shen, and G. Chen, Physical Review B **78**, 115303 (2008).

[55] R. Incardone, T. Emig, and M. Krüger, EPL (Europhysics Letters) **106**, 41001 (2014).

[56] C. Otey and S. Fan, Phys. Rev. B **84**, 245431 (2011).

[57] C. R. Otey, L. Zhu, S. Sandhu, and S. Fan, Journal of Quantitative Spectroscopy and Radiative Transfer **132**, 3 (2014).

[58] X. Liu, R. Zhang, and Z. Zhang, Applied Physics Letters **103**, 213102 (2013).

[59] S.-A. Biehs, M. Tschikin, and P. Ben-Abdallah, Physical review letters **109**, 104301 (2012).

[60] B. Liu and S. Shen, Physical Review B **87**, 115403 (2013).

[61] H. Callen and T. Welton, Physical Review **83**, 34 (1951).

[62] L. D. Landau and E. M. Lifshitz, (1969).

[63] W. Eckhardt, Opt. Commun. **41**, 305 (1982).

[64] D. B. Hough and L. R. White, Advances in Colloid and Interface Science **14**, 3 (1980).

[65] E. D. Palik, *Handbook of optical constants of solids*, Vol. 3 (Academic press, 1998).

[66] E. Lifshitz, Sov. Phys. JETP **2**, 73 (1956).

[67] A. Narayanaswamy and G. Chen, Physical Review B **77**, 075125 (2008).

[68] NIST Chemistry WebBook (NIST standard reference data), http://webbook.nist.gov/chemistry/.

[69] K. Sasihithlu and A. Narayanaswamy, Phys. Rev. B **83**, 161406 (2011).

[70] C. Fosco, F. C. Lombardo, and F. D. Mazzitelli, Phys. Rev. D **84**, 105031 (2011).